

The dark nature of GRB 130528A and its host galaxy

S. Jeong¹, A. J. Castro-Tirado^{1,2}, M. Bremer³, J. M. Winters³, J. Gorosabel^{1,4,5}, S. Guziy⁶, S. B. Pandey⁷, M. Jelínek¹, R. Sánchez-Ramírez¹, Ilya V. Sokolov^{8,9}, N. V. Orekhova^{10,11}, A. S. Moskvitin¹², J. C. Tello¹, R. Cunniffe¹, O. Lara-Gil¹, S. R. Oates¹, D. Pérez-Ramírez¹³, J. Bai^{14,15}, Y. Fan^{14,15,16}, C. Wang^{14,15,16}, and I. H. Park¹⁷

¹ Instituto de Astrofísica de Andalucía (IAA-CSIC), Glorieta de la Astronomía s/n, E-18008, Granada, Spain.
e-mail: sjeong@iaa.es

² Unidad Asociada Departamento de Ingeniería de Sistemas y Automática, E.T.S. de Ingenieros Industriales, Universidad de Málaga, Spain.

³ Institute de Radioastronomie Millimétrique (IRAM), 300 rue de la Piscine, 38406 Saint Martin d' Hères, France.

⁴ Unidad Asociada Grupo Ciencias Planetarias UPV/EHU-IAA-CSIC, Departamento de Física Aplicada I, E.T.S., Ingeniería, Universidad del País Vasco UPV/EHU, Bilbao, Spain.

⁵ Ikerbasque, Basque Foundation for Science, Bilbao, Spain.

⁶ Nikolaev National University, Nikolska 24, Nikolaev 54030, Ukraine.

⁷ Aryabhata Research Institute of Observational Sciences, Manora Peak, Nainital - 263 002, India.

⁸ Terskol Branch of Institute of Astronomy Russian Academy of Sciences, Elbrus ave., 81/33, Tyrnyauz, Kabardino-Balkaria Republic, 361623, Russia.

⁹ Saint Petersburg State University, Universitetskiy ave 28, Petrodvorets, Saint Petersburg, 198504, Russia.

¹⁰ Petrozavodsk State University, Lenin Str., 33, 185910, Petrozavodsk, Russia.

¹¹ Open joint stock company, "Scientific Production Corporation System of Precision Instrument Making", Aviamotornaya, 53, Moscow, Russia.

¹² Special Astrophysical Observatory, Nizhniy Arkhyz, Zelenchukskiy region, Karachai-Cherkessian Respublic, 369167, Russia.

¹³ Universidad de Jaén, Campus Las Lagunillas, s/n, Jaén, Spain.

¹⁴ Yunnan Observatories, Chinese Academy of Sciences, Kunming 650011, China.

¹⁵ Key Laboratory for the Structure and Evolution of Celestial Objects, Chinese Academy of Sciences, Kunming 650011, China.

¹⁶ University of Chinese Academy of Sciences, Beijing 100049, China.

¹⁷ Department of Physics, Sungkyunkwan University, Suwon, Korea.

Received; accepted Aug 20, 2014

ABSTRACT

Aims. We study the dark nature of GRB 130528A through multi-wavelength observations and conclude that the main reason for the optical darkness is local extinction inside of the host galaxy.

Methods. Automatic observations were performed at the Burst Optical Observer and Transient Exploring System (BOOTES)-4/MET robotic telescope. We also triggered target of opportunity (ToO) observations at Observatorio de Sierra Nevada (OSN), IRAM Plateau de Bure Interferometer (PdBI) and Gran Telescopio Canarias (GTC + OSIRIS). The host galaxy photometric observations in optical to near-infrared (nIR) wavelengths were achieved through large ground-based aperture telescopes, such as 10.4m Gran Telescopio Canarias (GTC), 4.2m William Herschel Telescope (WHT), 6m Bolshoi Teleskop Alt-azimutalnyi (BTA) telescope, and 2m Liverpool Telescope (LT). Based on these observations, spectral energy distributions (SED) for the host galaxy and afterglow were constructed.

Results. Thanks to millimetre (mm) observations at PdBI, we confirm the presence of a mm source within the XRT error circle that faded over the course of our observations and identify the host galaxy. However, we do not find any credible optical source within early observations with BOOTES-4/MET and 1.5m OSN telescopes. Spectroscopic observation of this galaxy by GTC showed a single faint emission line that likely corresponds to [OII] 3727Å at a redshift of 1.250 ± 0.001 , implying a star formation rate (SFR)(M_{\odot}/yr) $> 6.18 M_{\odot}/\text{yr}$ without correcting for dust extinction. The probable line-of-sight extinction towards GRB 130528A is revealed through analysis of the afterglow SED, resulting in a value of $A_V^{GRB} \geq 0.9$ at the rest frame; this is comparable to extinction levels found among other dark GRBs. The SED of the host galaxy is explained well ($\chi^2/d.o.f.=0.564$) by a luminous ($M_B=-21.16$), low-extinction ($A_V=0$, rest frame), and aged (2.6 Gyr) stellar population. We can explain this apparent contradiction in global and line-of-sight extinction if the GRB birth place happened to lie in a local dense environment. In light of having relatively small specific SFR (SSFR) $\sim 5.3 M_{\odot}/\text{yr} (L/L^*)^{-1}$, this also could explain the age of the old stellar population of host galaxy.

Key words. gamma-ray bursts: individual - technique: photometric: spectroscopic - cosmology: observations

1. Introduction

Since the launch of the *Swift*, $\sim 78\%$ (667/856 as of Apr 1, 2014) of observed Gamma-ray Bursts (GRBs)¹, were detected accurately and rapidly by the *Swift* X-ray telescope (XRT). Among

them $\sim 73\%$ (488/667) of GRBs were detected by the *Swift* UV/optical telescope (UVOT) or ground-based telescopes at UV/optical/IR wavelengths, but UV/optical/IR emission was not detected in 20-27% of observed GRBs (see also Melandri et al. 2012; Greiner et al. 2011), despite deep searches during several hours by ground facilities. Events lacking UV/optical/IR emis-

¹ http://swift.gsfc.nasa.gov/archive/grb_table/

sion are dubbed "dark GRBs" (Groot et al. 1998) with GRB 970111 being the first such case (Castro-Tirado et al. 1997; Gorosabel et al. 1998).

Currently dark GRBs are defined as those events having no UV/optical afterglow but also a relatively low optical-to-X-ray flux ratio (see Jakobsson et al. 2004 and van der Horst et al. 2009). Plausible causes for dark GRBs, such as observational bias, high level of extinction within the galaxy, Lyman- α cut-off (for high redshift bursts) and intrinsically low UV/optical fluxes are claimed, although a combination of two or three causes is likely (also discussed by Rol et al. 2005; Fynbo et al. 2001). The number of well-observed dark GRBs and their hosts is continually being increased thanks to well-targeted ground-based ToO campaigns, which enable us to gain better insight into the nature of GRBs and their environments. Moreover, future space-based missions, Ultra-Fast Flash Observatory (UFFO)-pathfinder/*Lomonosov*, and UFFO might be helpful to understand the dark nature of GRBs using the early optical follow-up within several seconds after GRB onset (Park et al. 2013; Jeong et al. 2013).

Recent studies have shown that dust extinction inside of the host galaxy might be the probable cause of darkness; the GRB is generated in a denser environment compared with optically bright events (De Pasquale et al. 2003; Perley et al. 2009; Melandri et al. 2012). The prompt properties of dark GRBs at rest frame do not differ with optically bright events, but interestingly, the average X-ray luminosity (unabsorbed X-ray flux at rest frame) of dark bursts is slightly higher, although the observed optical flux is slightly lower (see Fig. 4 in Melandri et al. 2012). A significant correlation between intrinsic X-ray column density and β_{OX} has been pointed out by Campana et al. (2012), and dark GRBs ($\beta_{OX} < 0.5$, Jakobsson et al. 2004) have been shown to have a moderately high column density in comparison to optically bright events.

Host galaxies that harbour dark GRBs are interesting as a study for unbiased samples of star-bursts galaxies in the universe related with SFR (Christensen et al. 2004). Some hosts of dark GRBs trace a sub-population of massive star-burst galaxies, which differ from the main GRB host galaxy population (Rossi et al. 2012). Krühler et al. (2011) report similar results, in that the hosts of the dustiest afterglows have diverse properties but are on average redder, more luminous, and massive in comparison to hosts of optically bright events (see also Hunt et al. 2014). Perley et al. (2013) also deduced similar results by investigating 23 dust obscured *Swift* GRBs. It suggests that their hosts are more massive, about an order of magnitude, compared with unobscured GRBs at similar redshifts.

On May 28, 2013, at 16:41:23 UT, the *Swift* Burst Alert Telescope (BAT) triggered and located the "North pole" GRB (D'Elia et al. 2013; Goad et al. 2013). The BAT light curve is multiple-peaked with a duration of about 84 s and exhibited a peak count rate of ~ 5500 counts/s in the 15-350 keV range at ~ 8 s after the trigger. The time-averaged spectrum from $T_0+0.12$ to 79.34 s was fitted by a power law with an exponential cutoff with a photon index 1.39 ± 0.19 , E_{cutoff} of 118.3 ± 79.7 keV and total fluence of $5.1 \pm 0.2 \times 10^{-6}$ erg/cm² in the 15-150 keV band (D'Elia et al. 2013; Cummings et al. 2013).

The *Swift*/XRT began observing the field at 64.9 s after the BAT trigger and found a bright, fading uncatalogued X-ray source (D'Elia et al. 2013). An astrometrically corrected X-ray position was reported later, RA(J2000)=09^h18^m0.12^s and Dec(J2000)=+87°18'03.7" with an uncertainty of 1.8 arcsec (radius, 90% confidence, Goad et al. 2013). Initial XRT spectral analysis resulted in a column density of $3.6 \pm 0.6 \times 10^{21}$ cm⁻²

(90 % confidence, Melandri et al. 2013) in excess of the galactic value at 8.5σ (5.2×10^{20} cm⁻², Kalberla et al. 2005), which shows a high equivalent hydrogen column density N_H resembling GRB 051022 (Castro-Tirado et al. 2007). The *Swift*/UVOT started follow-up observations 75 s after the BAT trigger, however, it did not detect any credible afterglow candidate within the XRT error circle down to 21.7 mag in the white filter (D'Elia et al. 2013; De Pasquale & D'Elia 2013). This encouraged ground-based observations at several different wavelengths. The 0.4m telescope at ISON-Kitab Observatory commenced observations 20 min after the BAT trigger with no optical counterpart being reported at a 3σ limit > 19.1 mag (unfiltered images of 30 s exposure, see Volnova et al. 2013).

In this paper, we discuss the reason for the dark nature of GRB 130528A, using our dataset from the optical to mm wavelengths. The structure of our paper is as follows: in Section 2, we describe our multi-wavelength observations and data reduction. In Section 3, we discuss the observational results, which lead us to consider GRB 130528A as a dark GRB, as well as the host galaxy properties, before summarising our conclusions in Section 4.

2. Observations and data reduction

2.1. Photometric observations in optical/near-infrared wavelength

Following the detection by *Swift*/BAT and XRT and the non-detection by UVOT, an autonomous search by BOOTES-4/MET was performed prior to a follow-up program with several ground-based telescopes. Early time optical observations were carried out at the BOOTES-4/MET robotic telescope in Lijiang, China (Castro-Tirado et al. 2012), which automatically responded to the GRB alert with observations being conducted on May 28, 17:52:42 UT, which are ~ 1.1 h after the *Swift*/BAT trigger ($T_0=16:41:23$ UT) in the clear and r-band filters (120 s and 180 s exposures, respectively). The field calibration was achieved using GTC deep observations (see below). We also triggered the 1.5m OSN located in the Sierra Nevada mountain range in the *I*-band (600 s exposure), and the field calibration was conducted using USNO B1.0 catalogue.

Broadband observations in the optical and nIR for the potential host galaxy were conducted to produce a SED. Observations were performed using various large aperture ground-based telescopes, such as the GTC in r- and i-filters that ranges from ~ 3.4 d to ~ 312 d after the burst. The z-band host galaxy observations were imaged with the 2.0m LT equipped with the the IO:O instrument during three consecutive nights starting on Apr 4, 2014. The z-band field calibration was carried out using the transformation formulas given by Jordi et al. (2006) and the GTC r&i-band secondary standards. A B-band observation was conducted with the 6m BTA telescope with SCORPIO located in the Zelenchuksky District on the north side of the Caucasus Mountains in southern Russia. The nIR observations in *J* and *K_S* pass-bands using director discretionary time (DDT) were carried out at 4.2m WHT equipped with LIRIS on Dec 23, 2013 with seeing $\sim 0.8-1.2''$. The field was calibrated using faint standards, FS130 and FS131. The images were reduced, accounting for flat-field and sky background, using the standard method within the IRAF. The bias subtraction was performed automatically at the time of data saving. The log of optical/nIR observations are summarised in Table 1. To determine the photometric magnitudes, we used aperture photometry with the DAOPHOT routine in IRAF².

² <http://iraf.noao.edu>

Table 1. Photometric observations at the GRB 130528A field at optical/nIR wavelengths. No correction for Galactic extinction is applied.

Start Time (UT) (mid exposure)	T-T ₀ (mid days)	Telescope/ Instrument	Filter Grism	Exposure time (seconds)	Magnitude (AB)
May 28, 2013, 17:52:42.438	0.050	BOOTES-4/MET	clear	120	>19.7 (3 σ)
May 28, 2013, 17:54:46.385	0.052	BOOTES-4/MET	Sloan r	180	>19.8 (3 σ)
May 28, 2013, 17:57:50.198	0.054	BOOTES-4/MET	clear	120	>19.7 (3 σ)
May 29, 2013, 20:41:42.640	1.167	1.5m OSN	<i>I</i>	600	>23.0 (3 σ)
Jun 1, 2013, 03:04:50.211	3.409	10.4m GTC	Sloan i	100 \times 9	22.87 \pm 0.08
Jun 1, 2013, 02:41:32.625	3.417	10.4m GTC	Sloan r	60 \times 3	23.28 \pm 0.01
Jun 2, 2013, 02:56:40.228	4.427	10.4m GTC	Sloan i	100 \times 1	22.74 \pm 0.15
Dec 23, 2013, 05:45:16.011	208.554	4.2m WHT	<i>J</i>	9 \times 197	21.63 \pm 0.35
Dec 23, 2013, 06:59:02.247	208.610	4.2m WHT	<i>K_S</i>	3 \times 432	21.43 \pm 0.25
Dec 31, 2013, 21:57:12.000	217.219	6m BTA	<i>B</i>	300 \times 8	23.41 \pm 0.10
Apr 05, 2014, 22:37:42.667	312.247	2.0m LT	Sloan z	300 \times 36	22.41 \pm 0.15

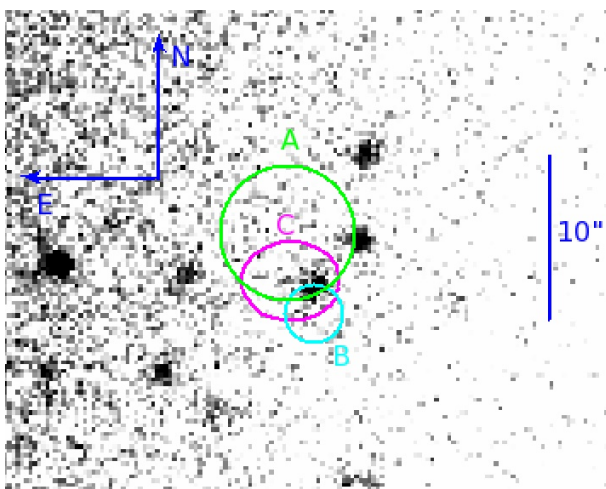


Fig. 1. The Sloan i-band median combined image ($T_{exp}=9 \times 100$ s) of the field of GRB 130528A taken with the 10.4m GTC on Jun 1, 2013. Circle A & B represents the XRT error circles in 4.1 arcsec (D’Elia et al. 2013) and 1.8 arcsec (Goat et al. 2013) radius, respectively. The ellipse C shows the mm detection beam size by PdBI (see Sect. 2.2 in this paper). It clearly points out the putative host galaxy of GRB 130528A by confirming a mm afterglow with a signal-to-noise ratio of ~ 4 (at 86.7 GHz). The measured i-band magnitude is 22.87 ± 0.08 in AB system.

2.2. Millimetre observations

Millimetre observations were obtained between ~ 1.33 d and ~ 3 d after the GRB onset on May 29, 2013 and Jun 02, 2013, via our on-going ToO program at PdBI in the French Alps (Guilloteau et al. 1992) with a compact five antenna D configuration. Observations were conducted at 86.7 GHz with a beam size of $5.95'' \times 4.81''$. Data reduction was carried out using the GILDAS³ software.

2.3. Host galaxy spectroscopy

Optical spectroscopy with OSIRIS at the 10.4m GTC started on Jun 02, 2013, which is ~ 3.4 d after the trigger, using the R1000B (3×600 s exposures) and R500R grism (1×600 s exposures). The 1.2'' slit was positioned on the location of the host galaxy, and a 2×2 binning mode was used for data acquisition. The obtained spectra were reduced and calibrated following standard procedures using custom tools based in IRAF and Python. The

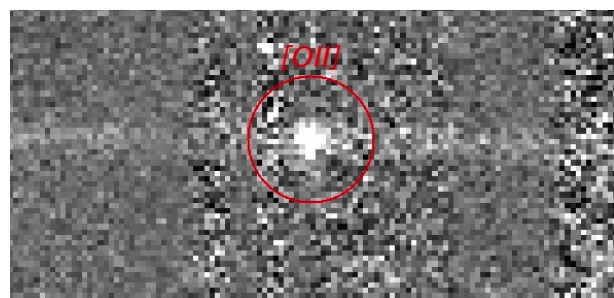


Fig. 2. The proposed [OII] 3727 emission line in the 2D spectrum of the host galaxy for GRB 130528A. The emission line lies at 8500\AA , implying a redshift 1.250. The 1D spectrum cannot be properly extracted due to its faintness. We determined the line flux using photometry, $48 \pm 7.0 \times 10^{-18}$ ergs/s/cm².

standard spectrophotometric stars, Feige92 and GD140, were used for flux calibration (for R1000B and R500R, respectively, with a 2.5'' slit). We corrected flux of slit losses for all the spectra using the photometry of the corresponding acquisition images.

3. Results and discussions

3.1. No optical/nIR afterglow detections and host galaxy observations at the optical/nIR wavelengths

No plausible optical/nIR transient was detected down to 19.7 mag ($T_0+1.1$ h, clear) at BOOTES-4/MET and 23.0 mag ($T_0+1.17$ d, *I*-band) at 1.5m OSN telescopes. The potential host galaxy was first revealed using our on-going ToO program at 10.4m GTC in the Sloan r and i-bands and is shown in Fig. 1. It has 22.9 mag in the i-band and 23.3 mag in the r-band. The z-band brightness is revealed with 22.4 mag by LT. The nIR data was reduced under the IRAF routine and resulted in magnitudes of 21.6 mag and 21.4 mag in *J* and *K_S*, respectively. The BTA B-band observation gave a magnitude of 23.4 mag. All magnitudes are given in Table 1 and are presented in the AB system (vega to AB offset is following Fukugita et al. 1995).

3.2. Afterglow detection at mm

From the mm observations between ~ 1.33 d and ~ 3 d after the GRB, we clearly confirm a mm afterglow with a signal-to-noise ratio of ~ 4 (at 86.7 GHz) at the position of the putative host galaxy, thus confirming the association. The mm source was not detected in the second dataset, implying a signifi-

³ <http://www.iram.fr/IRAMFR/GILDAS>

Table 2. mm afterglow flux densities measured at the Plateau de Bure Interferometer.

Start Time (UT)	End Time (UT)	Configuration	Flux density [mJy]	Frequency [GHz]
May 29, 2013, 23:33	May 30, 2013, 01:42	5Dq	0.38 ± 0.10	86.7
Jun 02, 2013, 13:13	Jun 02, 2013, 15:03	5Dq	$< 0.07 \pm 0.09$	86.7

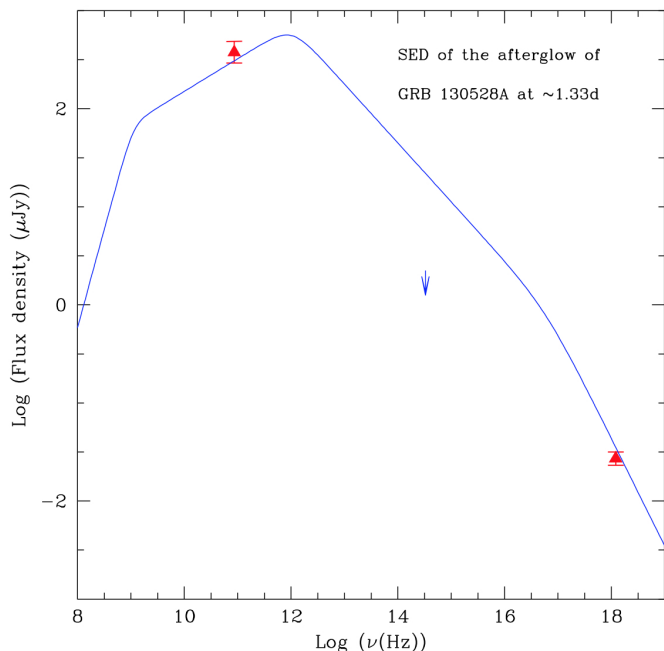


Fig. 3. The SED of GRB 130528A afterglow at 1.33 days. A model is overplotted with the observed data, assuming $\nu_a=1.1 \times 10^9$ Hz, $\nu_m=1.1 \times 10^{12}$ Hz, $\nu_c=6 \times 10^{16}$ Hz, $F_{\nu_{max}}=700 \mu\text{Jy}$, $p=2.2$, and a smoothing parameter $s=3$ in the case of the ISM model $\nu_a < \nu_m < \nu_c$. The red arrows represent observed flux in the radio and X-ray at 1.33 days. The blue arrow shows the *I*-band upper limit observed by 1.5m OSN at a similar epoch. The low upper limit can be explained by a significant extinction in the line-of-sight.

icant fading of the afterglow flux between the two observations. The phase center coordinates are RA(J2000)= $09^h 18^m 02.22^s$ and Dec(J2000)= $+87^\circ 18' 05.7''$ in the outskirts of the XRT error circle (D’Elia et al. 2013). The position coincides well with the astrometrically corrected X-ray position (Goat et al. 2013), which enabled us to propose the identification of the host galaxy of GRB 130528A.

3.3. Predicted optical brightness from the afterglow SED

We determined the expected brightness for the optical afterglow by following the standard fireball model (Sari et al. 1998). At the time of the radio observation by the PdBI, (i.e., $T_0+1.33$ d), we took the X-ray flux at a similar epoch from the XRT light curve. The over plot of the afterglow SED model (see Fig. 3) was constructed assuming the following parameters: $\nu_a=1.1 \times 10^9$ Hz, $\nu_m=1.1 \times 10^{12}$ Hz, $\nu_c=6 \times 10^{16}$ Hz, $F_{\nu_{max}}=700 \mu\text{Jy}$, $p=2.2$, and a smoothing parameter $s=3$ in the slow cooling regime (Sari et al. 1999), showing the best overlap to the observed mm and X-ray data. We also constrained the parameters of the blast wave as $E_{52}=10.9$, $n=0.004 \text{ cm}^{-3}$, $\epsilon_e=0.02$, and $\epsilon_b=0.01$ by the assumed model parameters using equations 27-30 of Wijers & Galama (1999). We checked the appropriation of p using the time sliced

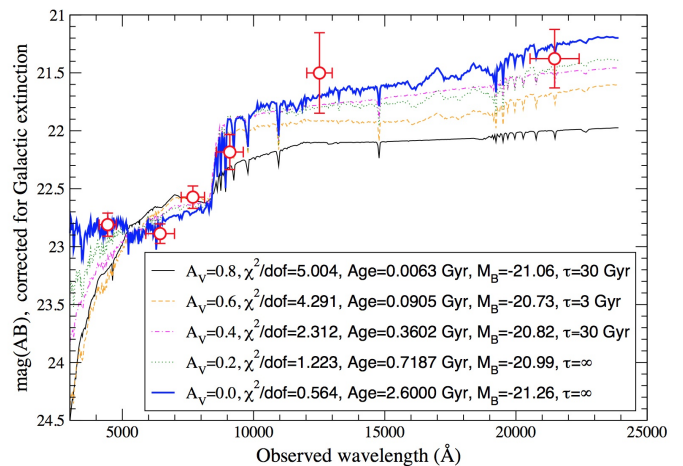


Fig. 4. The SED of GRB 130528A host galaxy in the B,r,i,z,J, and K_S bands. The AB magnitudes are corrected considering for the Galactic extinction $E(B-V)=0.144$ (Schlafly & Finkbeiner 2011). The thick line shows the best fit ($\chi^2/d.o.f.=0.564$) achieved with $A_V=0$, a stellar population with an age of 2.6 Gyr, $M_B=-21.16$, and Solar metallicity. The rest of the lines show the evolution of the SED fit when A_V increases gradually from 0 to 0.8. As seen, the fit gets worse when A_V grows.

XRT spectrum tool⁴ on the timescale that displays less spectral evolution, such as $T_0+22091 - T_0+115883$ s. The fit shows the photon index to be $2.02^{+0.44}_{-0.40}$, resulting in a large uncertainty in p . Therefore, we used a universal value of $p=2.2$ for the energy distribution of the electrons. The XRT spectral tool also gave a intrinsic value for excess absorption to be $N_{H,i}=3.7^{+2.6}_{-2.0} \times 10^{21} \text{ cm}^{-2}$. The modelled SED can be used to estimate the amount of extinction by dust in the line-of-sight. The predicted magnitude in *I*-band at $T_0=1.33$ days is ~ 20.4 mag (vega), and the upper limit produced by 1.5m OSN was 22.5 mag (vega). Therefore, it implies a minimum extinction $A_{I,min} \sim 0.8$ mag ($A_{V,min} \sim 0.9$) at rest frame (after galactic extinction correction by Schlafly & Finkbeiner 2011). Another independent measurement of the expected UV/optical extinction can be obtained from the X-ray absorption to dust-extinction ratio, $N_{H,X}/A_V$, following Schady et al. (2010). The X-ray absorption $N_{H,X}$ of GRB 130528A with rest frame, which is produced using the “zTBabs” model within Xspec (Evans et al. 2009), is $N_{H,X}=2.79 \pm 2.61 \times 10^{22} \text{ cm}^{-2}$. Using the mean values of $N_{H,X}/A_V=3.3 \times 10^{22}$, 3.4×10^{22} and $2.1 \times 10^{22} \text{ cm}^{-2}$ for the different extinction models (Small Magellanic Cloud (SMC), Large Magellanic Cloud (LMC), and Milky Way (MW), see Schady et al. 2010), A_V was found to be 0.84, 0.82, and 1.32 mag for SMC, LMC, and MW, respectively. These values are consistent with the previous findings from the afterglow SED.

3.4. Redshift determination and the star-formation rate

The single emission line at 8500 \AA in the GTC spectra likely corresponds with [OII] 3727 \AA at a redshift $z=1.250 \pm 0.001$, how-

⁴ http://www.swift.ac.uk/xrt_spectra

ever, due to the low SNR of the spectrum, the 1D projection of the optical spectrum could not be extracted. The [OII] line in 2D spectrum is shown in Fig. 2. The emission line flux is $48 \pm 7.0 \times 10^{-18}$ ergs/s/cm², as measured by line photometry. Using this value, we can derive a lower limit on the SFR by applying the calibration of Kennicutt (1998), which is $\text{SFR}(M_{\odot}/\text{yr}) = 1.4 \pm 0.4 \times 10^{41} L_{[\text{OII}]}$. At a redshift $z=1.25$, the corresponding luminosity distance is $D_L=8.768$ Gpc (assuming $H_0=71$ km s⁻¹Mpc⁻¹, $\Omega_m=0.27$, and $\Omega_{\Lambda}=0.73$). Taking the lower limit for the optical extinction into account, this implies $\text{SFR}(M_{\odot}/\text{yr}) > 6.18 M_{\odot}/\text{yr}$. It signifies a $\text{SSFR} \sim 5.3 M_{\odot}/\text{yr} (L/L^*)^{-1}$ (assuming $M_B^* = -21$), which is a low value compared to other SSFRs estimated in long GRB host galaxies (Christensen et al. 2004).

3.5. The host galaxy spectral energy distribution

Broadband observations were matched using the Hyperz code (Bolzonella et al. 2000) to synthetic SED templates based on the GISSSEL 98 library (Bruzual & Charlot 1993). The time evolution of the SFR for each template is represented by an exponential model, which is $\text{SFR} \propto \exp(-t/\tau)$, where τ is the SFR timescale. Eight values of τ were explored (0,1,2,3,5,15,30, and ∞ Gyr) and the initial mass function (IMF) given by Miller & Scalo (1979) was assumed. The impact of the metallicity (which is expected to be minor, as tested by Bolzonella et al. 2000) was considered, using both solar metallicity and evolving metallicity templates, which assumed an instantaneous recycling of heavy elements. For each τ value, the extinction (A_V) and the dominant stellar population age were left as free parameters. The host galaxy magnitudes were corrected by Galactic reddening by assuming an $E(B-V)=0.144$ (Schlafly & Finkbeiner 2011).

To check the stability of our SED solution, we first let the redshift vary from 0.1 to 5. The photometric redshift yields $z=1.397^{+0.097}_{-0.085}$ (68% confidence interval) are fairly consistent with the spectroscopic redshift. Thus, the redshift of the SED fit was fixed to the spectroscopic redshift value (see Sect. 3.4). As displayed in Fig. 4, the best fit is obtained with a Solar metallicity and intrinsically bright ($M_B=-21.16$) and low extinction ($A_V \sim 0$) galaxy, which dominated by an evolved (age ~ 2.6 Gyr, $\tau = \infty$) stellar population. If the metallicity is assumed to be evolving, the derived values are qualitatively equivalent ($A_V \sim 0$, Age ~ 1.434 Gyr, $\tau=5$ Gyr, $M_B=-21.03$, $\chi^2/d.o.f.=0.754$). Due to the lack of other emission lines within our spectral window, we cannot constrain the metallicity of the host galaxy.

This is not the first case where a low (global) extinction galaxy harbours a highly extinguished afterglow (for instance GRB 000210 or GRB 000418; Gorosabel et al. 2003a,b). This apparent contradiction might be explained by line-of-sight dust that is probably close to the progenitor birth place. However, we have to be cautious about the uniqueness of the SED solution. As a sanity check of a possible age-extinction degeneracy, we studied the SED fit evolution when the host A_V ranged from $A_V=0$ to $A_V=0.8$ (see Fig. 4). As expected, the dominant stellar population age decreases when A_V grows. However, the impoverishment of the fit is clear when A_V increases; A_V values larger than 0.8 (not shown in the plot for visual clarity) provide an even worse fit. We, thus, conclude that the $A_V=0$ SED fit is a solid solution.

Unfortunately for the redshift of the host, it is impossible that the H_{α} and H_{β} emission lines do fall in the *JHK*-band atmospheric windows, so no Balmer decrement (and hence direct host extinction spectroscopic check) measurement would be possible from the ground.

The derived high τ and old stellar population age are con-

sistent with low SSFR (see Sect. 3.4 in this paper), therefore a feasible picture could be one in which the main episode(s) of star-formation of this host remains constant in time or slowly decays in intensity. The host of GRB 130528A also has a red colour, $(R-K)_{AB}=1.54$ (Sloan *r*-filter is transformed to the *R* using Lupton 2005⁵), this colour excess yields a similar characteristic to the hosts of the dustiest afterglows, as shown in Krühler et al. (2011).

4. Conclusions

In this work, we have shown that the darkness of the long duration "dark" GRB 130528A was likely due to the high absorption close to the GRB birth place, lying in a galaxy at $z=1.25$, which is pinpointed thanks to the mm detection by PdBI. Based on optical/nIR host galaxy observations at GTC, WHT, BTA, and LT, we infer that the GRB 130528A occurred in a low extinction ($A_V \sim 0$), aged (dominate stellar population of 2.6 Gyr), red $((R-K)_{AB}=1.54)$, and luminous ($M_B=-21.16$) host. However, this host galaxy seems different with respect to the main body of long-GRB hosts (Christensen et al. 2004) and is consistent with the characteristics of the dustiest hosts shown by the latest statistical studies (Perley et al. 2013; Rossi et al. 2012). Through mm and nIR observations by PdBI and 1.5m OSN at similar epochs, we infer the relative extinction along the line-of-sight towards the GRB 130528A, which is $A_V^{GRB} \geq 0.9$ mag in rest frame. We also show that this result is consistent with the expected UV/optical extinction from rest frame $N_{H,X}$. The inconsistency between the significant extinction expected from the afterglow SED model and low external extinction determined from the host galaxy SED could be reconciled if the GRB was located in a high density environment, such as a local molecular cloud.

Acknowledgements. This work is partly based on observations carried out with the 0.6m BOOTES-4/MET in China, with the Gran Telescopio Canarias (GTC), installed in the Spanish Observatorio del Roque de los Muchachos of the Instituto de Astrofísica de Canarias, in the island of La Palma and with the IRAM Plateau de Bure Interferometer. IRAM is supported by INSU/CNRS (France), MPG (Germany) and IGN (Spain). The Liverpool Telescope is operated on the island of La Palma by Liverpool John Moores University in the Spanish Observatorio del Roque de los Muchachos of the Instituto de Astrofísica de Canarias with financial support from the UK Science and Technology Facilities Council. Alexander Moskvitin supported by Research Program OFN-17 of the Division of Physics, Russian Academy of Sciences. We acknowledge the support of F. J. Aceituno (OSN observatory) and the Spain's Ministerio de Ciencia y Tecnología through Projects AYA2009-14000-C03-01/ESP, AYA2011-29517-C03-01, AYA2012-39362-C02-02, and Creative Research Initiatives of NRF in Korea (Research Center of MEMS Space Telescope). This work made use of data supplied by the UK *Swift* Science Data Centre at the University of Leicester. We acknowledge the use of public data from the *Swift* data archives and the service provide by the gamma-ray burst Coordinates Network (GCN) and BACODINE system, maintained by S. D. Barthelmy. We thank the referee for carefully reading this manuscript and providing valuable comments, which helped improve the text substantially. We also acknowledge valuable discussions and comments from Z. Lucas Uhm.

References

- Bolzonella, M., Miralles, J.-M., & Pelló, R. 2000, *A&A*, 363, 476
- Bruzual, G. & Charlot, S. 1993, *ApJ*, 405, 538
- Campana, S., Salvaterra, R., Melandri, A., et al. 2012, *MNRAS*, 421, 1697
- Castro-Tirado, A. J., Bremer, M., McBreen, S., et al. 2007, *A&A*, 475, 101
- Castro-Tirado, A. J., Gorosabel, J., Heidt, J., et al. 1997, *IAUC*, 6598
- Castro-Tirado, A. J., Jelínek, M., Gorosabel, J., et al. 2012, *BASI Conf. Ser.*, 7, 313
- Christensen, L., Hjorth, J., & Gorosabel, J. 2004, *A&A*, 425, 913
- Cummings, J. R., Barthelmy, S. D., Baumgartner, W. H., et al. 2013, *GCN Circ.*, 14718

⁵ <http://classic.sdss.org/dr5/algorithms/sdssUBVRITransform.html>

- De Pasquale, M. & D'Elia, V. 2013, GCN Circ., 14721
- De Pasquale, M., Piro, L., Perna, R., et al. 2003, ApJ, 592, 1018
- D'Elia, V., Burrows, D. N., Gronwall, C., et al. 2013, GCN Circ., 14711
- Evans, P. A., Beardmore, A. P., Page, K. L., et al. 2009, MNRAS, 397, 1177
- Fukugita, M., Shimasaku, K., & Ichikawa, T. 1995, PASP, 107, 945
- Fynbo, J. U., Jensen, B. L., Gorosabel, J., et al. 2001, A&A, 369
- Goad, M., Osborne, J., Beardmore, A., & Evans, P. 2013, GCN Circ., 14714
- Gorosabel, J., Castro-Tirado, A., Wolf, C., et al. 1998, A&A, 339, 719
- Gorosabel, J., Christensen, L., Hjorth, J., et al. 2003a, A&A, 400, 127
- Gorosabel, J., Klose, S., Christensen, L., et al. 2003b, A&A, 409, 123
- Greiner, J., Krühler, T., Klose, S., et al. 2011, A&A, 526, A30
- Groot, P. J., Galama, T. J., van Paradijs, J., et al. 1998, 493
- Guilloteau, S., Delannoy, J., Downes, D., et al. 1992, A&A, 262, 624
- Hunt, L. K., Palazzi, E., Michałowski, M. J., et al. 2014, A&A, 565, A112
- Jakobsson, P., Hjorth, J., Fynbo, J. P. U., et al. 2004, ApJ, 617, L21
- Jeong, S., Nam, J. W., Ahn, K. B., et al. 2013, OpEx, 21, 2263
- Jordi, K., Grebel, E. K., & Ammon, K. 2006, A&A, 460, 339J
- Kalberla, P. M. W., Burton, W. B., Hartmann, D., et al. 2005, A&A, 440, 775
- Kennicutt, R. C. 1998, ARA&A, 36, 189
- Krühler, T., Greiner, J., Schady, P., et al. 2011, A&A, 534, A108
- Melandri, A., Sbarufatti, B., D'Avanzo, P., et al. 2012, MNRAS, 421, 1265
- Melandri, A., Sbarufatti, B., Stroh, M., et al. 2013, GCN Circ., 14716
- Miller, G. E. & Scalo, J. M. 1979, A&AS, 41, 513
- Park, I. H., Brandt, S., Budtz-Jørgensen, C., et al. 2013, NJP, 15, 023031
- Perley, D. A., Cenko, S. B., Bloom, J. S., et al. 2009, ApJ, 138, 1690
- Perley, D. A., Levan, A. J., Tanvir, N. R., et al. 2013, ApJ, 778, 128P
- Rol, E., Wijers, R. A. M. J., Kouveliotou, C., Kaper, L., & Kaneko, Y. 2005, ApJ, 624, 868
- Rossi, A., Klose, S., Ferrero, P., et al. 2012, A&A, 545, A77
- Sari, R., Piran, T., & Halpern, J. P. 1999, ApJ, 519, L17
- Sari, R., Piran, T., & Narayan, R. 1998, ApJ, 497, L17
- Schady, P., Page, M. J., Oates, S. R., et al. 2010, MNRAS, 401, 2773
- Schlafly, E. F. & Finkbeiner, D. P. 2011, ApJ, 737, 103S
- van der Horst, A. J., Kouveliotou, C., Gehrels, N., et al. 2009, ApJ, 699, 1087
- Volnova, A., Litvinenko, E., Molotov, I., & Pozanenko, A. 2013, GCN Circ., 14712
- Wijers, R. A. M. J. & Galama, T. J. 1999, ApJ, 523, 177